# Direct Observation and Measurement of Mobile Charge Carriers in a Monolayer Organic Semiconductor on a Dielectric Substrate

**Yeping Jiang,[†,‡] Qiong Qi,[†] Rui Wang,[†] Jun Zhang,[†] Qikun Xue,[‡] Chen Wang,[†] Chao Jiang,[†] and Xiaohui Qiu[†,*]**

[†]National Center for Nanoscience and Technology, Beijing 100190, China, and [‡]Department of Physics, Tsinghua University, Beijing 100084, China

**ABSTRACT** We report the electrical characterization of a single layer of an organic semiconductor grown on a dielectric surface. The dynamic response of the charge carriers in the monolayer film of pentacene was characterized through the electrostatic interactions between an electric force microscope (EFM) probe and pentacene islands of various sizes. These islands were formed *in situ* by segmenting a coalesced pentacene monolayer into separated regions. The size-dependent dielectric responses of the pentacene islands suggest that mobile charges exist in the organic monolayer. Local capacitance spectroscopy revealed that the charge carriers in the p-type pentacene monolayer could be depleted at high bias voltages, enabling a further determination of the charge-carrier concentration in the organic semiconductor ultrathin film.

**KEYWORDS:** electric force microscopy (EFM) · organic semiconductor · pentacene · charge carrier · monolayer film · dielectric substrate

Organic molecules are commonly used as functional components in flexible, lightweight, and cost-effective electronic devices.[1,2] For a variety of $\pi$-conjugated molecules, field-effect mobilities that surpass that of polymorphous silicon have been achieved.[3,4] Recently, n-type molecular semiconductors on chemically modified gate dielectric surfaces have been used to control the polarity and density of charge carriers in organic thin film transistors (OTFTs).[5] This shows the potential for applications based on organic electronic materials.

OTFTs are interface devices in which charge transport occurs within the first few layers of molecules that are in close contact with the gate insulator.[6−9] However, the electrical properties of these ultrathin layers remain largely unknown because of the lack of reliable characterization techniques. For pentacene on dielectric substrates, it is difficult to obtaining high-quality films with large-scale structural uniformity and integrity. The polycrystalline morphology of pentacene impedes the application of spatially averaged measurements and complicates the interpretation of electrical transport characteristics.[10,11] Although photoelectron spectroscopy has been used to investigate the band structures of organic ultrathin film grown on conductive substrates,[12] direct measurements of the electrical properties of organic materials on gate dielectrics are necessary for an in-depth understanding of the fundamental processes that affect the operation and performance of OTFT devices.

Here we present an electrical characterization of a single layer of an organic semiconductor grown on a dielectric surface using an approach based on electric force microscopy (EFM). EFM is a versatile and spatially precise method for studying the electrostatic inhomogeneities in crystalline grains at grain boundaries,[11,13−16] the potential profile near organic heterojunctions,[17,18] and at organic/electrode interfaces.[19−21] We used the imaging and lithography capabilities of EFM to investigate the dynamic response of the charge carriers in a monolayer film of pentacene. By measuring the electrostatic interaction between the EFM probe and the pentacene islands of various sizes in the monolayer, we showed that mobile charges exist in the organic monolayer on the oxide substrate. The capacitance−voltage characteristics of the pentacene monolayer further allow for a quantitative measurement of the charge-carrier concentration in the organic semiconductor ultrathin film.

## RESULTS AND DISCUSSION

A schematic of the experimental setup is shown in Figure 1a. Figure 1b shows a

* Address correspondence to xhqiu@nanoctr.cn.

Received for review February 24, 2011 and accepted July 8, 2011.

**Published online July 08, 2011**
**10.1021/nn200760r**

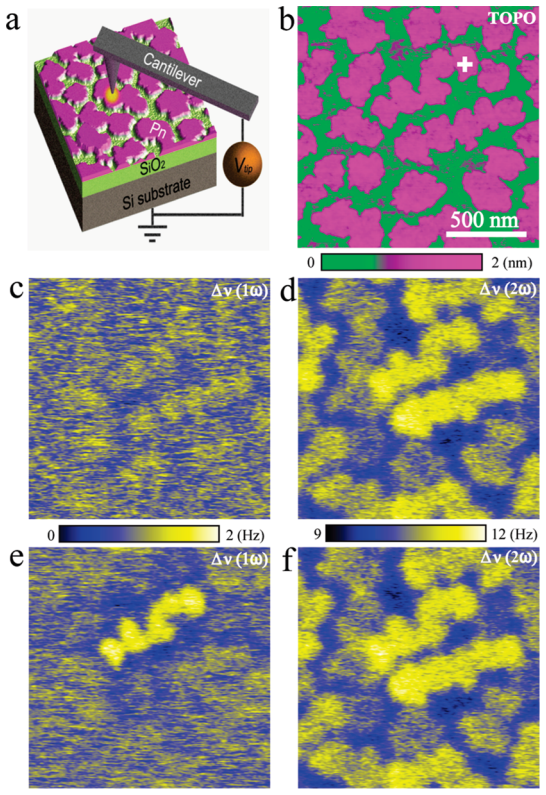


**Figure 1. (a) Schematic of the experimental setup. (b) Topographic, (c) $\Delta\nu(1\omega)$, and (d) $\Delta\nu(2\omega)$ images for the pentacene submonolayer grown on the $SiO_2$ substrate. All three images were acquired simultaneously. Images of (e) $\Delta\nu(1\omega)$ and (f) $\Delta\nu(2\omega)$ after charge injection at the pentacene grain marked with a cross in (b). The tip lift height was 10 nm when the $\Delta\nu(1\omega)$ and $\Delta\nu(2\omega)$ images were acquired. The tip was biased at 0.5 V to zero out the contact potential between the tip and substrate in the measurements. The *Z*-scale bar for (b) corresponds to a height variation of 2 nm.**

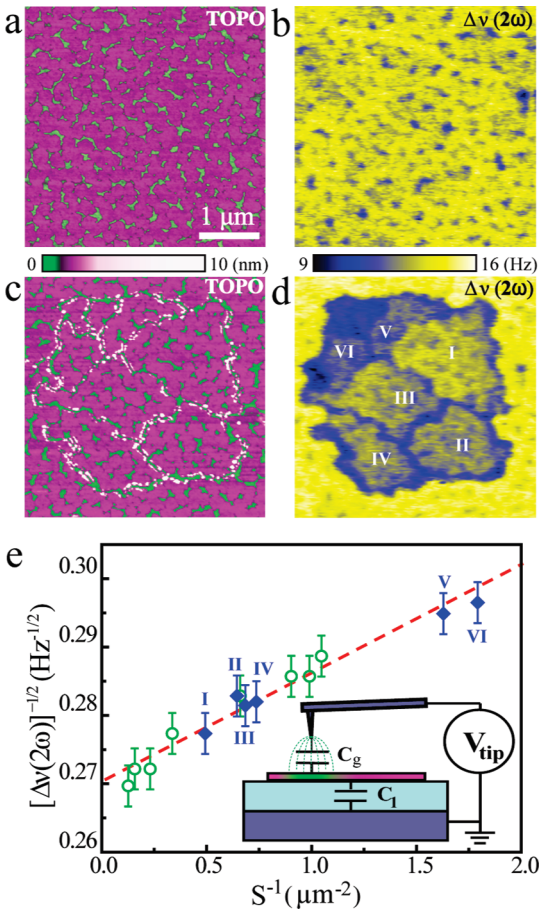


**Figure 2. (a) Topographic and (b) $\Delta\nu(2\omega)$ images of the pentacene monolayer grown on the $SiO_2$ substrate. (c) Coalesced pentacene film was segmented into multiple islands by physically removing the molecules at the crystalline boundaries. (Some residue was present at the edge of the pentacene islands after the lithography process.) The *Z*-scale bar indicates a height variation of 10 nm. (d) Image of $\Delta\nu(2\omega)$ corresponding to (c). (e) Plots of $\Delta\nu^{-1/2}(2\omega)$ *vs* $S^{-1}$ measured for pentacene islands of various sizes. The data shown by solid squares were measured on the corresponding islands shown in (d). The data shown by hollow circles correspond to the islands formed during the intermediate steps in the lithography process. The dashed line is the curve fitted using the series capacitor model shown in the inset. The error bars denote the $\Delta\nu(2\omega)$ signal fluctuations measured at different locations on each pentacene island. The areas of the segmented regions were calculated using the topographic image and the SPM software package.**

topographic image of the pentacene submonolayer film on a degenerately doped Si substrate with a 250 nm thick $SiO_2$ layer, exhibiting a polycrystalline morphology resulting from the Stranski–Krastanov growth mode.[22,23] The molecular orientation and grain morphology of the first layer of pentacene depend on the pentacene–substrate interactions.[9] The micrometer-sized grains have a height of 2 nm, which indicates the near-vertical orientation of pentacene molecules on the $SiO_2$ substrate.[8] At higher coverage, the pentacene grains grew laterally and interconnected with each other. The multilayer pentacene film had a field-effect mobility of 1.0 $cm^2\ V^{-1}\ s^{-1}$ in the saturation region.[24]

Figure 1c,d shows EFM images that were taken simultaneously with the topographic image, which is shown in Figure 1b. The EFM signals, $\Delta\nu(1\omega)$ and $\Delta\nu(2\omega)$, measure the electric force gradients associated with the charges/dipoles and the polarization responses of the samples, respectively.[25,26] The difference in $\Delta\nu(1\omega)$ for the pentacene grains and bare $SiO_2$ surface (Figure 1c) can be attributed to the induced dipole at the pentacene/$SiO_2$ interface. This dipole is induced by the difference in the work functions of the materials.[11,13] The spatial variation in $\Delta\nu(1\omega)$ for the different pentacene islands is insignificant despite the variation in the crystallographic orientation of the crystalline grains. These findings are similar to those of Chen *et al.*[13] However, in contrast to the homogeneity seen in Figure 1c, the value of $\Delta\nu(2\omega)$ varied significantly for the pentacene islands (Figure 1d). Because the $\Delta\nu(2\omega)$ EFM signal corresponds to the polarizability of the samples underneath the EFM probe,[25] it is somewhat surprising to find that the

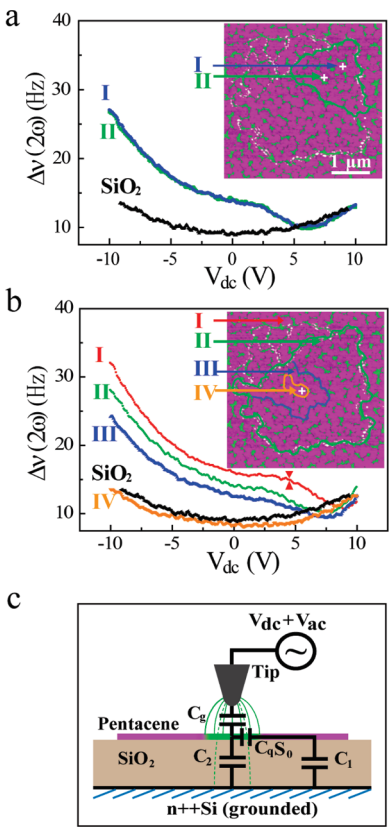


**Figure 3. (a) Spectra of $\Delta\nu(2\omega)-V_{dc}$ acquired at two different locations (marked by crosses in the inset) on an isolated pentacene island and on the bare $SiO_2$ substrate. The EFM response of the bare $SiO_2$ substrate was periodically measured to serve as a proxy for tip cleanliness during the experiment. The inset is a topographic image of a monolayer pentacene film. (b) Evolution of $\Delta\nu(2\omega)-V_{dc}$ characteristics after a sequence of lithography steps on the pentacene monolayer. All spectra were acquired at the same location (marked by a cross in the inset). Curve I was taken before the lithography process. Curves II, III, and IV are the spectra measured after sequentially forming islands II, III, and IV, respectively. The spectrum recorded for $SiO_2$ is shown for comparison. The point indicated by the pair of arrows on curve I is defined as the turning point voltage where $\Delta\nu(2\omega)$ decreases abruptly. (c) Schematic of the capacitive circuit of the tip/pentacene monolayer/$SiO_2$/Si junction.**

crystalline pentacene grains have varying dielectric responses. A correlation with crystalline orientation was not evident for the observed variance.[6]

Following ref 14, we performed local charge injection by bringing a biased EFM tip into close contact with the isolated pentacene islands. From Figure 1e, it can be seen that the charge-injected island exhibited sharp contrast in the $\Delta\nu(1\omega)$ image. The uniform appearance of the $\Delta\nu(1\omega)$ signal in the island indicates a charge delocalization.[27] Although there was significant variation in $\Delta\nu(1\omega)$, little change in $\Delta\nu(2\omega)$ was observed for the charge-injected pentacene islands (Figure 1f).

Figure 2a,b shows topographic and $\Delta\nu(2\omega)$ images for a coalesced pentacene monolayer in which the crystalline grains of pentacene were interconnected. The grain boundaries were not distinguishable in either of the images (Figure 2a or b). We used the EFM tip to make a series of controlled scratches on the film at specific locations. The pentacene monolayer film was segmented into discrete islands that had various sizes and shapes[28] (Figure 2c). Although the tip only removed a small amount of pentacene molecules at the edge of each of the islands, pronounced changes were observed in the corresponding regions in $\Delta\nu(2\omega)$ image (Figure 2d). The corresponding $\Delta\nu(1\omega)$ image is shown as Figure S2c in Supporting Information. The $\Delta\nu(2\omega)$ signal for isolated pentacene islands was dramatically reduced in comparison with that of a continuous film, which is made of interconnected crystalline pentacene grains. The $\Delta\nu(2\omega)$ signal for each of the pentacene islands monotonically decreased with the island size, which can be seen in the plot in Figure 2e. The signals of the three smallest islands, which comprised only a few grains, were very small and not distinguishable from that of the $SiO_2$ substrate.

The capacitive interaction between the EFM probe and substrate, EFM $\Delta\nu(2\omega)$, is generally written as[25]

$$\Delta\nu(2\omega) = \frac{1}{4}\frac{\nu}{2k}\left(\frac{\partial^2 C}{\partial z^2}\right){V_{ac}}^2$$

where $\nu$ and $k$ are the resonant frequency and force constant of the EFM cantilever, respectively. $\partial^2C/\partial z^2$ is the second derivative of the capacitance of the tip−sample−substrate junction, $C$, with respect to the tip−substrate distance, $z$. The capacitance, $C$, consists of the dielectric contribution of the pentacene film and the underlying $SiO_2$ layer. The pentacene monolayer has a thickness of 2 nm and an approximate nominal dielectric constant of 4.[29] Therefore, its contribution to the total tip−sample−substrate capacitance is negligible compared with that from the 250 nm thick $SiO_2$ layer. We do not expect that the value of $\Delta\nu(2\omega)$ measured for the pentacene monolayer would be distinguishable from the bare $SiO_2$ substrate if the polarization of the pentacene molecule was the only effect taken into account.

We believe that the variation in the value of $\Delta\nu(2\omega)$ observed for the different pentacene islands resulted from the mobile charge carriers present in the organic thin film. As shown in the inset of Figure 2e, the pentacene layer can be modeled as a conductive plate. This plate forms two capacitors in series, $C_g$ and $C_1$, with the EFM tip and the degenerately doped Si substrate, respectively. Because of the small lift height used in the experiment,[30] the force gradient signal we measure and the capacitance charge effect mainly arise from the interaction between the tip apex and sample.[25,31] The capacitance, $C_g$, arises from the limited region beneath the tip apex.[32]

When the tip voltage with respect to the substrate is modulated, the voltage applied between the tip and

pentacene film, $V_{tp}$, can be written as[33]

$$V_{tp} = V_{ac}[1 + (C_g/C_1)]^{-1} \quad (1)$$

Here, $V_{ac}$ is the modulated voltage applied to the EFM tip; $C_1 = C_0S$; $C_0$ is the oxide capacitance per unit area;[34] and $S$ is the total area of the pentacene island comprising all interconnected grains. $C_g$ can be treated as a constant for a given EFM tip and same measurement conditions. We expect that $C_g \ll C_1$ because the EFM tip apex is much smaller than the pentacene islands. Thus, the EFM $\Delta\nu(2\omega)$ signal can be written as

$$\Delta\nu(2\omega) = \frac{1}{4}\frac{\nu}{2k}C_g''V_{tp}^2 = \left(\frac{1}{4}\frac{\nu}{2k}V_{ac}^2C_g''\right)[1 + (C_g/C_0)S^{-1}]^{-2} \quad (2)$$

We define $\alpha = (1/4)(\nu/2k)V_{ac}^2C_g''$ for the following discussion.

The linear dependence of $[\Delta\nu\ (2\omega)]^{-1/2}$ on $S^{-1}$, which is derived in eq 2, agrees well with the experimental data shown in Figure 2e. This validates the above-mentioned capacitance model and provides evidence of the mobile carriers in the pentacene film. The $\Delta\nu(2\omega)$ signal arises from the effect of the charge carriers flowing into and out of the region underneath the EFM tip apex when the modulated electric field is applied. Larger pentacene islands form larger capacitors with the ground Si substrate, which results in an increased voltage drop at the tip−pentacene junction. Therefore, the $\Delta\nu(2\omega)$ signal is enhanced.

The nature of the mobile charges in the pentacene film was investigated using $\Delta\nu(2\omega)$ spectroscopy. Figure 3a shows the $\Delta\nu(2\omega)-V_{dc}$ characteristics for various positions on an isolated pentacene island and on the bare $SiO_2$ substrate.[35] The two spectra measured on the pentacene island have similar features that are different from those of the substrate. This confirms the delocalization of the charge carriers in the interconnected crystalline grains. The minima for $\Delta\nu(2\omega)$ was obtained in the spectra of pentacene for a positive tip voltage. Similar behavior was also seen in the spectra acquired from the other pentacene islands of various sizes (Figure 3b). The spectra are rather flat around zero gate voltage. This explains why the $\Delta\nu(2\omega)$ signal of the crystalline island (Figure 1f) barely increased after hole injection. (An increase of surface potential by 15 mV was measured, therefore the amount of injected hole was very limited.)

The EFM tip is believed to act simultaneously as a scanning gate[36] and a microscopic capacitance meter during the $\Delta\nu(2\omega)-V_{dc}$ characterization. When a bias voltage $V_{dc}$ is applied to the tip, the charge carriers in the film redistribute in response to the non-uniform electric field near the tip apex. The variation in the local carrier density underneath the tip, $\delta n$, causes a change in the chemical potential of $\delta\mu$ relative to the original band structure. This lateral band bending in the pentacene layer leads to a shift in the vacuum level between the charged area, $S_0$, and the surrounding region.[37] This effect becomes more pronounced when the film has a finite density of states (DOS).

In capacitance measurement, an additional capacitance $C_q = e^2\delta n/\delta\mu$ in series with the geometry capacitance was introduced to account for the extra energy required to accommodate charges besides the electrostatic energy.[38,39] Whereas the energy comes from electron−electron interactions in carbon nanotube and graphene,[40,41] known as the quantum capacitance effect,[38,42] the energy in pentacene monolayer may derive from the finite carrier density of states in the organic thin film.[43] In our experiment, we also suggest that the accommodation of the charge carriers in the pentacene monolayer is limited by the finite DOS at the Fermi level in the film. On the other hand, the EFM responses of the pentacene film, such as the spectral line shape and depletion voltage, did not vary appreciably when the AC frequency of the tip voltage was varied in the range of 200 to 800 Hz, indicating that the gate-dependent capacitance signal is not originated from the carrier-density-dependent mobility in this frequency range.

An equivalent circuit model of the system is shown in Figure 3c. $C_qS_0$ is the capacitance of the tip-gated pentacene area, $S_0$. $C_qS_0$ is in series with the geometry capacitances $C_g$ and $C_1$. In this case, $C_1$ is the ground capacitance of the charged pentacene region. $C_1$ can be ignored for the pentacene islands that contain many interconnected grains, which produce a large geometric capacitance with respect to the substrate. The penetrating electric field can be simulated by the addition of a capacitance, $C_2$, in parallel with $C_q$ and $C_1$. In this case, $C_2 = C_0S_0$ is the oxide capacitance of the area below the gated pentacene. $C_2$ is much smaller than $C_qS_0$ and $C_1$.

In the capacitance model described by eqs 1 and 2, we assumed that at zero gate voltage the pentacene monolayer has a sufficient DOS near the Fermi level to accommodate the charges induced by the electric field of the EFM tip. The thin film behaves as a metal-like layer that efficiently screens the transverse electric field. When a considerably higher tip voltage is applied, the capacitance of the organic layer ($C_qS_0$) may be significantly reduced and must be taken into account. Equation 2 can be further written as

$$\Delta\nu(2\omega) = \alpha[1 + C_g/(C_qS_0) + (C_g/C_0)S^{-1}]^{-2} \quad (3)$$

The linear fit (in Figure 2e) yields a slope of $\alpha^{-1/2}(C_g/C_0)$ and a $y$-axis intercept of $\alpha^{-1/2}(1 + C_g/C_qS_0)$. Thus, $(C_g^{-1} + C_q^{-1}S_0^{-1})^{-1}$ is determined to be $8 \times 10^{-18}$ F. The scenario described in eq 2 is equivalent to the case when $C_g \ll C_q(0)S_0$, where $C_q(0)$ is the capacitance at zero gate voltage.

The $\Delta\nu(2\omega)-V_{dc}$ spectra shown in Figure 3a,b are analogous to the $I_{ds}/V_{gate}$ characteristics of field-effect transistors.[44,45] When the value of $\Delta\nu(2\omega)$ approaches that of the bare substrate at a positive voltage, the mobile carriers are depleted, which suggests that the pentacene monolayer is a p-type semiconductor.[4]

Earlier studies have shown that the presence of holes at a zero gate bias arises from the electron acceptor states in the band gap close to the HOMO-derived valence band. These states most likely form as a result of the hydroxyl groups at the semiconductor/dielectric interface.[5] When a positive tip voltage is applied, the chemical potential of the p-type organic film shifts away from the valence band, which decreases the mobile hole density. We defined the voltage corresponding to the minimum value of $\Delta\nu(2\omega)$ as $V_{deplete}$. At this voltage, the carrier density of pentacene at the gated region approaches zero [$C_q \sim 0$]. Namely, the film becomes locally nonconductive. The modulated electric field emanating from the EFM tip can penetrate through the organic layer and cause charge accumulation in the heavily doped Si substrate. The situation can be simulated by placing the two capacitances, $C_g$ and $C_2$, in series.

The condition, $C_g \ll C_q(0)S_0$, is readily satisfied because $V_{deplete}$ is much larger than the induced chemical potential shift in the pentacene layer.[46] Therefore, the tip voltage mainly imposes on the geometric capacitance ($C_g$) before the turning point (indicated by the arrows in Figure 3b). $C_g$ is estimated to be $8 \times 10^{-18}$ F. From this, we calculated that the carrier density at zero gate voltage in the pentacene monolayer was approximately $1.3 \times 10^{12}/cm^2$. Our results on single-layer pentacene are similar to those of transport measurements on pentacene TFT,[44,47,48] implying that the carrier transport in OTFT takes place in the few molecular layers closest to the gate dielectric. The noncontact capacitance approach proposed here provides a versatile tool in thin film investigation, circumventing the contact problems in standard scanning capacitance microscopy or transport measurements.

## CONCLUSIONS

The electrical characteristics of a monolayer pentacene film were investigated using EFM. The mobile carriers were shown to exist in the organic ultrathin film through a measurement of the capacitive interaction between the EFM probe and pentacene islands. The capacitance of the organic layer was measured using capacitance spectroscopy, which enabled a quantitative measurement of charge-carrier concentration in the organic film. The approach presented in this study circumvents the electrostatic complexity of the metal/organic contacts that are used in conventional transport measurements, allowing for a direct characterization of the electrical properties of organic ultrathin films deposited on dielectric substrates. Future experiments conducted in vacuum and at a variable temperature may further explain the mechanisms that govern charge transport in organic electronic materials.

## EXPERIMENTAL SECTION

Pentacene thin films were prepared *via* the thermal evaporation of pentacene (purity >99%, Aldrich Co.) on degenerately n-doped Si(100) substrates with a 250 nm $SiO_2$ layer (Northeast Microelectronics Research Institute) in a high-vacuum evaporator (Auto-306, BOC-Edwards Co.). The deposition rate was 0.02 nm/s at a base pressure of $7 \times 10^{-5}$ Pa. The substrates were kept at room temperature during the deposition. The samples were transferred immediately to a scanning probe microscope (Dimension 3100, Veeco Metrology) that was housed in a nitrogen chamber. The EFM measurements were performed using a two-pass scan technique. The first pass maps the topography of the sample for each scan line using a standard tapping mode. The oscillation amplitude of the tip was about 26 nm. During the second pass, the probe scans over the sample surface at a lift height of $\Delta h$ (10 nm) with respect to the sample topography. Simultaneously, a modulated voltage, $V_{tp} = V_{dc} + V_{ac}\sin(\omega t)$, was applied to the Pt/Ir-coated tip (SCM-PIC, Veeco Metrology). The voltage was measured with respect to the grounded substrate (Figure 1a), and the amplitude of the tip was reduced to about 16 nm. For all of the EFM measurements, $V_{ac}$ = 2 V and a modulation frequency of 500 Hz was used. The $1\omega$ and $2\omega$ components of the resonant frequency shift signal of the cantilever were demodulated *via* lock-in amplifiers and recorded simultaneously with the topographic images through a signal-access module to yield the corresponding EFM $\Delta\nu(1\omega)$ and $\Delta\nu(2\omega)$ images.[26] The $\Delta\nu(1\omega)$ and $\Delta\nu(2\omega)$ images were taken at a tip lift height of 10 nm with feedback off. The oscillation amplitude of the tip was calibrated using the amplitude *versus z* spectroscopy on the silicon surface.

*Acknowledgment.* This work was supported by the National Basic Research Program of China (No. 2007CB936802) and the Chinese Academy of Sciences (No. KJCX-YW-M04). The authors also acknowledge the financial support of the National Science Foundation of China (No. 20973046).

*Supporting Information Available:* Additional details and figures. This material is available free of charge *via* the Internet at http://pubs.acs.org.

## REFERENCES AND NOTES

1. Douvas, A. M.; Makarona, E.; Glezos, N.; Argitis, P.; Mielczarski, J. A.; Mielczarski, E. Polyoxometalate-Based Layered Structures for Charge Transport Control in Molecular Devices. *ACS Nano* **2008**, *2*, 733–742.
2. Klauk, H.; Zschieschang, U.; Pflaum, J.; Halik, M. Ultralow-Power Organic Complementary Circuits. *Nature* **2007**, *445*, 745–748.
3. Coropceanu, V.; Cornil, J.; da Silva, D. A.; Olivier, Y.; Silbey, R.; Bredas, J. L. Charge Transport in Organic Semiconductors. *Chem. Rev.* **2007**, *107*, 926–952.
4. Dimitrakopoulos, C. D.; Malenfant, P. R. L. Organic Thin Film Transistors for Large Area Electronics. *Adv. Mater.* **2002**, *14*, 99–117.

5. Chua, L.-L.; Zaumseil, J.; Chang, J.-F.; Ou, E. C. W.; Ho, P. K. H.; Sirringhaus, H.; Friend, R. H. General Observation of n-Type Field-Effect Behaviour in Organic Semiconductors. *Nature* **2005**, *434*, 194–199.
6. Dinelli, F.; Murgia, M.; Levy, P.; Cavallini, M.; Biscarini, F.; de Leeuw, D. M. Spatially Correlated Charge Transport in Organic Thin Film Transistors. *Phys. Rev. Lett.* **2004**, *92*, 116802.
7. Facchetti, A.; Yoon, M. H.; Marks, T. J. Gate Dielectrics for Organic Field-Effect Transistors: New Opportunities for Organic Electronics. *Adv. Mater.* **2005**, *17*, 1705–1725.
8. Fritz, S. E.; Martin, S. M.; Frisbie, C. D.; Ward, M. D.; Toney, M. F. Structural Characterization of a Pentacene Monolayer on an Amorphous $SiO_2$ Substrate with Grazing Incidence X-ray Diffraction. *J. Am. Chem. Soc.* **2004**, *126*, 4084–4085.
9. Yang, H. C.; Shin, T. J.; Ling, M. M.; Cho, K.; Ryu, C. Y.; Bao, Z. N. Conducting AFM and 2D GIXD Studies on Pentacene Thin Films. *J. Am. Chem. Soc.* **2005**, *127*, 11542–11543.
10. Pesavento, P. V.; Puntambekar, K. P.; Frisbie, C. D.; McKeen, J. C.; Ruden, P. P. Film and Contact Resistance in Pentacene Thin-Film Transistors: Dependence on Film Thickness, Electrode Geometry, and Correlation with Hole Mobility. *J. Appl. Phys.* **2006**, *99*, 094504.
11. Puntambekar, K.; Dong, J. P.; Haugstad, G.; Frisbie, C. D. Structural and Electrostatic Complexity at a Pentacene/Insulator Interface. *Adv. Funct. Mater.* **2006**, *16*, 879–884.
12. Kakuta, H.; Hirahara, T.; Matsuda, I.; Nagao, T.; Hasegawa, S.; Ueno, N.; Sakamoto, K. Electronic Structures of the Highest Occupied Molecular Orbital Bands of a Pentacene Ultrathin Film. *Phys. Rev. Lett.* **2007**, *98*, 247601.
13. Chen, L.; Ludeke, R.; Cui, X.; Schrott, A. G.; Kagan, C. R.; Brus, L. E. Electrostatic Field and Partial Fermi Level Pinning at the Pentacene−$SiO_2$ Interface. *J. Phys. Chem. B* **2005**, *109*, 1834.
14. Heim, T.; Lmimouni, K.; Vuillaume, D. Ambipolar Charge Injection and Transport in a Single Pentacene Monolayer Island. *Nano Lett.* **2004**, *4*, 2145–2150.
15. Jaquith, M.; Muller, E. M.; Marohn, J. A. Time-Resolved Electric Force Microscopy of Charge Trapping in Polycrystalline Pentacene. *J. Phys. Chem. B* **2007**, *111*, 7711–14.
16. Muller, E. M.; Marohn, J. A. Microscopic Evidence for Spatially Inhomogeneous Charge Trapping in Pentacene. *Adv. Mater.* **2005**, *17*, 1410–1414.
17. Matyba, P.; Maturova, K.; Kemerink, M.; Robinson, N. D.; Edman, L. The Dynamic Organic p−n Junction. *Nat. Mater.* **2009**, *8*, 672–676.
18. Slinker, J. D.; DeFranco, J. A.; Jaquith, M. J.; Silveira, W. R.; Zhong, Y. W.; Moran-Mirabal, J. M.; Craighead, H. G.; Abruna, H. D.; Marohn, J. A.; Malliaras, G. G. Direct Measurement of the Electric-Field Distribution in a Light-Emitting Electrochemical Cell. *Nat. Mater.* **2007**, *6*, 894–899.
19. Stoliar, P.; Kshirsagar, R.; Massi, M.; Annibale, P.; Albonetti, C.; de Leeuw, D. M.; Biscarini, F. Charge Injection across Self-Assembly Monolayers in Organic Field-Effect Transistors: Odd−Even Effects. *J. Am. Chem. Soc.* **2007**, *129*, 6477–6484.
20. Chen, L. W.; Cherniavskaya, O.; Shalek, A.; Brus, L. E. Photoinduced Interfacial Charging and "Explosion" of Monolayer Pentacene Islands. *Nano Lett.* **2005**, *5*, 2241–2245.
21. Silveira, W. R.; Marohn, J. A. Microscopic View of Charge Injection in an Organic Semiconductor. *Phys. Rev. Lett.* **2004**, *93*, 116104.
22. Pratontep, S.; Brinkmann, M.; Nuesch, F.; Zuppiroli, L. Correlated Growth in Ultrathin Pentacene Films on Silicon Oxide: Effect of Deposition Rate. *Phys. Rev. B* **2004**, *69*, 165201.
23. Ruiz, R.; Nickel, B.; Koch, N.; Feldman, L. C.; Haglund, R. F.; Kahn, A.; Family, F.; Scoles, G. Dynamic Scaling, Island Size Distribution, and Morphology in the Aggregation Regime of Submonolayer Pentacene Films. *Phys. Rev. Lett.* **2003**, *91*, 136102.
24. Qi, Q.; Jiang, Y. P.; Yu, A. F.; Qiu, X. H.; Jiang, C. Enhancement of Electrical Conductance for Pentacene Thin Film Transistor by Controlling an Initial Layer-by-Layer Growth Mode Directly on $SiO_2$ Insulator. *Jpn. J. Appl. Phys.* **2009**, *48*, 04C164.
25. Cherniavskaya, O.; Chen, L. W.; Weng, V.; Yuditsky, L.; Brus, L. E. Quantitative Noncontact Electrostatic Force Imaging of Nanocrystal Polarizability. *J. Phys. Chem. B* **2003**, *107*, 1525–1531.
26. Krauss, T. D.; Brus, L. E. Charge, Polarizability, and Photoionization of Single Semiconductor Nanocrystals. *Phys. Rev. Lett.* **1999**, *83*, 4840.
27. A potential increase of about 15 mV in the charged region was observed in the surface potential image (not shown), indicating that holes were injected into the pentacene island.
28. Care was taken to prevent the damage to the crystalline grains in the tip lithography process. The trace of the tip could be identified by the deposits along the scratch route.
29. Silinsh, E. A.; Capek, V. *Organic Molecular Crystals*; AIP Press: New York, 1994.
30. The height of cantilever is about 10 $\mu$m, while that of the tip apex is about 36 nm.
31. Sacha, G. M.; Saenz, J. J. Cantilever Effects on Electrostatic Force Gradient Microscopy. *Appl. Phys. Lett.* **2004**, *85*, 2610–2612.
32. The dimension of this charged area can be estimated to be about 200 nm in diameter, which is smaller than the pentacene grain size: the point charge model gives $r_1 \sim 45$ nm, $r_2 \sim 100$ nm, where $r_1$, $r_2$ are half-maximum radii in the charge density distribution and the integral charge density distribution, respectively. In our estimation, the tip apex−sample distance is 36 nm and the apex radius is 25 nm from vendor. Our finite-element analysis gives similar results (shown in Figure S1 of the Supporting Information).
33. Bockrath, M.; Markovic, N.; Shepard, A.; Tinkham, M.; Gurevich, L.; Kouwenhoven, L. P.; Wu, M. W.; Sohn, L. L. Scanned Conductance Microscopy of Carbon Nanotubes and $\lambda$-DNA. *Nano Lett.* **2002**, *2*, 187–190.
34. A simple plane capacitor model of $C_0 = \varepsilon_0\varepsilon/d$ ($\varepsilon \sim 4$ for $SiO_2$, $d \sim 250$ nm) gives $C_0 \sim 1.4 \times 10^{-16}$ F/$\mu$m$^2$.
35. The observed parabolic line shape of $\Delta\nu(2\omega)$ as a function of $V_{dc}$ can be interpreted as cantilever bending toward the substrate surface subjected to capacitive force, resulting in an increased tip−sample capacitance.
36. Finkelstein, G.; Glicofridis, P. I.; Ashoori, R. C.; Shayegan, M. Topographic Mapping of the Quantum Hall Liquid Using a Few-Electron Bubble. *Science* **2000**, *289*, 90–94.
37. Band bending cannot occur in the vertical direction because the monolayer film is much thinner than the screening length in a semiconductor material.
38. Luryi, S. Quantum Capacitance Devices. *Appl. Phys. Lett.* **1988**, *52*, 501–503.
39. Tal, O.; Rosenwaks, Y.; Preezant, Y.; Tessler, N.; Chan, C. K.; Kahn, A. Direct Determination of the Hole Density of States in Undoped and Doped Amorphous Organic Films with High Lateral Resolution. *Phys. Rev. Lett.* **2005**, *95*, 256405.
40. Hwang, E. H.; Hu, B. Y.-K.; Das Sarma, S. Density Dependent Exchange Contribution to $\partial\mu/\partial n$ and Compressibility in Graphene. *Phys. Rev. Lett.* **2007**, *99*, 226801.
41. Ilani, S.; Donev, L. A. K.; Kindermann, M.; McEuen, P. L. Measurement of the Quantum Capacitance of Interacting Electrons in Carbon Nanotubes. *Nat Phys* **2006**, *2*, 687–691.
42. Dultz, S. C.; Jiang, H. W. Thermodynamic Signature of a Two-Dimensional Metal-Insulator Transition. *Phys. Rev. Lett.* **2000**, *84*, 4689.
43. Celebi, K.; Jadhav, P. J.; Milaninia, K. M.; Bora, M.; Baldo, M. A. The Density of States in Thin Film Copper Phthalocyanine Measured by Kelvin Probe Force Microscopy. *Appl. Phys. Lett.* **2008**, *93*, 083308.
44. Pernstich, K. P.; Haas, S.; Oberhoff, D.; Goldmann, C.; Gundlach, D. J.; Batlogg, B.; Rashid, A. N.; Schitter, G. Threshold Voltage Shift in Organic Field Effect Transistors by Dipole Monolayers on the Gate Insulator. *J. Appl. Phys.* **2004**, *96*, 6431.
45. Yoon, M.-H.; Kim, C.; Facchetti, A.; Marks, T. J. Gate Dielectric Chemical Structure−Organic Field-Effect

Transistor Performance Correlations for Electron, Hole, and Ambipolar Organic Semiconductors. *J. Am. Chem. Soc.* **2006**, *128*, 12851–12869.
46. The gate voltage $V_{deplete}$ moves the chemical potential from the valence band edge to just above the acceptor energy level to deplete the hole donor. The acceptor states are within tens of millivolts of the valence band edge to contribute to room temperature conductivity. Thus the gate-induced chemical potential shift is much smaller than the gate voltage, indicating a relative much larger DOS compared to the gate capacitance $C_g$.
47. McDowell, M.; Hill, I. G.; McDermott, J. E.; Bernasek, S. L.; Schwartz, J. Improved Organic Thin-Film Transistor Performance Using Novel Self-Assembled Monolayers. *Appl. Phys. Lett.* **2006**, *88*, 073505.
48. Suárez, S.; Fleischli, F. D.; Schaer, M.; Zuppiroli, L. From Oxide Surface to Organic Transistor Properties: The Nature and the Role of Oxide Gate Surface Defects. *J. Phys. Chem. C* **2010**, *114*, 7153–7160.